Funicular analysis of ribbed masonry vaults: a case study

M. Bruggi[a]*, B.A. Lógó[b] and Z. Deák[c]

[a]*Department of Civil and Environmental Engineering, Politecnico di Milano, Milano, Italy;* [b]*Department of Engineering Geology and Geotechnics, Budapest University of Technology and Economics, Budapest, Hungary;* [c]*, Tripartitum Építész Műhely Ltd., Budapest, Hungary;*

*corresponding author, Department of Civil and Environmental Engineering, Politecnico di Milano, Milano, Italy, Piazza Leonardo da Vinci 32, Milan, Italy. E-mail: matteo.bruggi@polimi.it

Funicular analysis of ribbed masonry vaults: a case study

A numerical method is implemented to cope with the funicular analysis of ribbed masonry vaults under self-weight. A two-layer spatial network with given plan geometry is adopted to account for the load path in the overlying vault and in the supporting ribs. The minimization of the horizontal thrusts is formulated in terms of an independent set of force densities, and in the vertical coordinates of the restrained nodes. Constraints are enforced on the height of the nodes and on the sign of the force densities, to seek anti-funicular networks in equilibrium with the loading that lie within the envelope of the ribbed vault. A stellar masonry vault originally built in the ancient church of Tereske (Hungary) is investigated, comparing results achieved by using either single-layer or two-layer spatial networks.

Keywords: funicular analysis, masonry vaults, ribbed vaults, stellar vaults, historical constructions

1. Introduction

Funicular analysis is an application of the lower bound theorem of limit analysis that is extensively adopted to cope with the assessment of curved structures in masonry buildings, see e.g. Roca et al. (2010), Tralli et al. (2014), D'Altri et al. (2019). Among the others, limit analysis approaches for masonry vaults were developed in Milani et al. (2008), introducing a curved element to perform the kinematic limit analysis of masonry shells, in Baratta and Corbi (2011), investigating no-tension stress fields that fulfil not only equilibrium, but also compatibility with strains and fractures, and in Fraddosio et al. (2020), introducing a new numerical approach for the lower bound limit analysis of masonry vaults.

The assessment of arches and vaults through funicular analysis can be performed looking at statically indeterminate networks of forces with vertices and edges of given topology: supports are prescribed at the restrained nodes of the network; unrestrained ones are in equilibrium with the applied loads. Under the assumption of negligible tensile strength, unbounded compressive strength and infinite frictional resistance, an arch / vault may be regarded as safe when any funicular polygon / network exists that lies within its envelope, see Heyman (1966).

When the above assumptions apply, the safety of a vault that is acted upon by a set of given loads can be assessed by searching for networks of compressive forces that fulfill equilibrium and lie fully within the intrados and the extrados of the curved structure. It is possible to enforce a reduced geometry of the vault, with the aim of avoiding any stress concentration in compression. Alternatively, the network can be forced to lie within the middle one-third of the cross-section of the vault to search for solutions that minimize the arising of cracks. At the restrained nodes, vertical and horizontal reactions arise. The equilibrium of the abutments is performed accounting for these reversed actions.

Several numerical approaches have been proposed in the literature to address the automatic generation of funicular networks. Among the others, reference is made to the funicular analysis presented in O'Dwyer (1999), the Thurst Network Analysis (TNA) in Block and Ochsendorf (2007), Block and Lachauer (2014a), the approach by Andreu (2007), which implements the hanging strings analogy, and the derivation of thrust surfaces via polyhedral stress functions, see Fraternali (2010). Indeed, the generation of statically admissible stress fields plays a key role in the solution of the equilibrium of no-tension solids, see in particular the singular stress fields derived from the Airy's formulation in Angelillo et al. (2013, 2014).

The Thurst Network Analysis was originally conceived to exploit the concept of duality between the geometry of the funicular network (i.e. the layout of the branches as projected on the horizontal plane) and the internal forces (i.e. the proportional equilibrated set of horizontal forces along the relevant edges). It has been recently reformulated in Marmo and Rosati (2017) to reduce the computational effort by focusing on the primal grid and to cope with general loading conditions, see also Marmo et al. (2018, 2019).

The equilibrium of funicular networks can be conveniently handled through the force density method, i.e. writing the problem in terms of the ratio force-to-length in each branch of the network, see Schek (1974). As originally investigated in the literature for the case of vertical loads, independent sets of branches can be detected for networks with fixed plan geometry, see Block and Lachauer (2014b) and Cercadillo-García and Fernández-Cabo (2016). However, enforcing the nodes to lie within a prescribed range of heights (the masonry envelope) is not a trivial task from a numerical point of view.

To this goal, a multi-constrained minimization problem has been formulated and solved through mathematical programming in Bruggi (2020). The minimization of the horizontal thrusts is written in terms of an independent set of force densities, and in the vertical coordinates of the restrained nodes. Constraints are enforced on the sign of the force densities and on the height of the nodes. The latter set of constraints is linear in the vertical coordinates of the restrained nodes (direct variables), while it depends on the inverse of the force densities (reciprocal variables). Indeed, the adoption of sequential convex programming was ideally conceived to handle subsequent approximations of objective function and constraints in terms not only of direct variables, but also of reciprocal ones. This method has been preliminary tested on the

generation of funicular networks for curved structures, including a cross vault, a cloister vault, and a dome. None of these was endowed with ribs.

The debated issue on the static function of the ribs emerging from the intrados of cross vaults is extensively discussed in Di Pasquale (1996), where arguments in favor of their primary static role or their purely ornamental function are reviewed. As argued in Como (2016), in both the uncracked and cracked state, cross vaults undergo large forces along the diagonals: these forces may be supported by the vault itself (within the thickness of the groin), as in the Roman architecture, or by emerging elements, as in the Gothic ribbed vaults, see also Bertolesi et al. (2019). However, as reported e.g. in Grillanda et al. (2019), Roman constructors were probably aware of this force concentration, since they also strengthened groins by means of arches located at the intrados of the vault. In the same study, an in-depth numerical investigation on the statics of complex masonry stellar vaults is performed, using upper-bound limit analysis and non-linear finite elements. The thickness of the ribs is found to remarkably affect the ultimate bearing capacity of complex ribbed vaults. An extended numerical analysis based on the discrete element method has been performed in Lengyel and Bagi (2015), pointing out peculiar features of ribbed cross vaults.

In this contribution, the funicular analysis of ribbed masonry vault is dealt with, adopting the multi-constrained formulation above introduced. The implementation of two-layer spatial networks with given plan geometry is investigated to account for the load path in the overlying vault and in the supporting ribs. Numerical simulations and comparisons with conventional one-layer networks are reported, concerning a stellar masonry vault originally built in the ancient church of Tereske (Hungary) and acted upon by gravitational loads.

It must be remarked that the implemented method of funicular analysis assumes infinite frictional resistance. Therefore, it does not allow investigating the role of friction in the assessment of vaulted masonry structures. Among the others, Beatini et al. (2018) use non-smooth contact dynamic analyses to assess the role of frictional forces resisting tensile hoop forces in masonry domes, whereas Mousavian and Casapulla (2020) introduces a limit analysis approach for hemispherical domes composed of interlocking blocks considering non-isotropic sliding resistance. Reference is also made to Chen and Bagi (2020), where discrete element simulations are used to assess that dry (cohesionless) contact between compressed masonry layers allows carrying significant tension perpendicularly to the direction of compression, depending on the type of bond pattern.

Section 2 reports fundamentals of the numerical method, addressing its implementation for (single- or two- layer) networks with fixed plan projection and fully/partially restrained nodes. Section 3 introduces the case study, focusing on the geometry of the investigated vault and reporting some notes on the history and the building material. Section 4 collects the results achieved through the numerical simulations, whereas Section 5 provides final comments and reports on further research on the topic.

2. The numerical method

The developments contained in Bruggi (2020) are summarized in this section, focusing on the special case in which only vertical loads act on the vault.

The force density method (FDM) by Schek (1974) is used to handle the geometry of funicular networks that are in equilibrium with a set of vertical loads applied at the nodes. A cartesian reference system with axes x, y, and z is considered. At first, the equations that link dependent and independent branches in any network having fixed

projection onto the horizontal plane x, y are considered, see Block and Lachauer (2014b).

Instead of addressing grids that comprise only unrestrained nodes and fully restrained nodes, networks that also include partially restrained node are assumed in the following derivation and in the simulations presented next.

The horizontal equilibrium of the nodes which are unrestrained along the x or y direction may be gathered in the following system of equations:

$$\begin{bmatrix} \boldsymbol{C}_x^T diag(\boldsymbol{C}_s \boldsymbol{x}_{s0}) \\ \boldsymbol{C}_y^T diag(\boldsymbol{C}_s \boldsymbol{y}_{s0}) \end{bmatrix} \boldsymbol{q} = \begin{bmatrix} \boldsymbol{0} \\ \boldsymbol{0} \end{bmatrix}, \tag{1}$$

where $\boldsymbol{x}_{s0}$ and $\boldsymbol{y}_{s0}$ are the vectors of the given x and y coordinates, respectively, for the n_s nodes of the network; $\boldsymbol{C}_s$ is the connectivity matrix of the network; $\boldsymbol{C}_x$ and $\boldsymbol{C}_y$ are the subsets of $\boldsymbol{C}_s$ referring to nodes that are unrestrained along x and y, respectively; $\boldsymbol{q}$ is the vector of the m force densities, being m the number of branches in the network. Indeed, by applying Gauss-Jordan elimination to Eqn. (1), the r dependent force densities $\tilde{\boldsymbol{q}}$ may be re-written in terms of the m-r independent ones $\bar{\boldsymbol{q}}$ as:

$$\tilde{\boldsymbol{q}} = \boldsymbol{B}\bar{\boldsymbol{q}} + \boldsymbol{d}, \tag{2}$$

where $\boldsymbol{B}$ and $\boldsymbol{d}$ have known entries.

The vertical equilibrium of the n unrestrained nodes of the network reads:

$$\boldsymbol{C}_z^T \boldsymbol{Q} \boldsymbol{C}_z \boldsymbol{z} + \boldsymbol{C}_z^T \boldsymbol{Q} \boldsymbol{C}_{fz} \boldsymbol{z}_f = \boldsymbol{p}_z, \tag{3}$$

where $\boldsymbol{z}$ and $\boldsymbol{z}_f$ gather the vertical coordinates of the nodes which are unrestrained and restrained, respectively, along the z axis; $\boldsymbol{C}_z$ is the subset of $\boldsymbol{C}_s$ for the vertically unrestrained nodes and $\boldsymbol{C}_{fz}$ its complementary subset; $\boldsymbol{p}_z$ is the vector of the vertical point loads; $\boldsymbol{Q} = diag(\boldsymbol{q})$.

Following Bruggi (2020), a multi-constrained optimization problem is formulated in terms of the *m-r* independent force densities $\overline{\boldsymbol{q}}$ and the n_f vertical coordinates of the nodes restrained along the vertical direction $\boldsymbol{z}_f$:

$$
\begin{cases}
\min\limits_{\overline{\boldsymbol{q}},\ \boldsymbol{z}_f} f(\overline{\boldsymbol{q}}) & \\
s.t. \quad \tilde{\boldsymbol{q}} = \boldsymbol{B}\overline{\boldsymbol{q}} + \boldsymbol{d} & (4.1) \\
\boldsymbol{C}_z^T \boldsymbol{Q} \boldsymbol{C}_z \boldsymbol{z} + \boldsymbol{C}_z^T \boldsymbol{Q} \boldsymbol{C}_{fz} \boldsymbol{z}_f = \boldsymbol{p}_z & (4.2) \\
z_j(\overline{\boldsymbol{q}}, \boldsymbol{z}_f) \geq z_j^{min} \qquad j = 1 \dots n & (4.3) \\
z_j(\overline{\boldsymbol{q}}, \boldsymbol{z}_f) \leq z_j^{max} \qquad j = 1 \dots n & (4.4) \\
\tilde{q}_k \leq 0 \qquad k = 1 \dots r & (4.5) \\
\overline{q}_i \leq 0 \qquad i = 1 \dots m - r & (4.6) \\
z_{fh}^{min} \leq z_{fh} \leq z_{fh}^{max} \qquad h = 1 \dots n_f & (4.7) \\
 & (4.8)
\end{cases}
$$

A norm of the horizontal thrusts is adopted as objective function. In the above statement $f(\overline{\boldsymbol{q}}) = \sum \sqrt{R_{xl}^2 + R_{yl}^2}$, where R_{xl} and R_{yl} are the horizontal components of the reaction computed at the *l*-th node of those included in the sum. According to Heyman (1966), results achieved through the minimization of the thrust could be regarded as statically admissible load paths that are compatible with spreading supports. The objective function can be evaluated accounting for all the nodes restrained along any horizontal direction; alternatively, it includes only a reduced set of restrained nodes, thus providing a minimization that is limited to that subset. In the numerical simulations presented next, the norm of the horizontal thrusts will be computed along the perimeter of the vault, either including or excluding the corner nodes. In the latter case, lower values of the thrust are expected to arise along the top of the perimetral walls, at the cost of more stressed imposts.

By using the equilibrium in Eqn. (4.3) along with Eqn. (4.2), the vertical coordinates of the unrestrained nodes may be written in terms of the minimization unknowns, i.e. $\overline{\boldsymbol{q}}$ and $\boldsymbol{z}_f$; suitable constraints can be formulated to prescribe a lower and an upper limit for each one of the n unconstrained nodes, see Eqn. (4.4) and (4.5). Side constraints for

$\boldsymbol{z}_f$ are used to enforce similar prescriptions to the n_f restrained nodes, whose vertical coordinates are among the variables of the minimization problem, see Eqn. (4.8). It is worth remarking that Eqns. (4.4), (4.5) and (4.8) enforce the network to lie within the thickness of the vault by controlling all its nodes, both unrestrained and restrained ones. Constraints on the sign of the force density in each branch of the network are accounted for in Eqn. (4.6) and (4.7), to search for compression-only networks.

Due to its peculiar form, the optimization problem in Eqn. (4) can be efficiently solved through techniques of sequential convex programming that were originally conceived to handle large scale multi-constrained formulations of structural optimization. In a stress-constrained minimum weight problem of truss design, cross-sections are sought such that the volume is minimized and strength constraints are fulfilled. In a statically determinate truss, the objective function is linear in the unknowns, whereas the constrained stress may be written in terms of the inverse of the unknowns. Dealing with the funicular polygon of an arch acted upon by vertical loads, it may be shown that the thrust is linear in the independent force density $\bar{q}$, whereas the vertical coordinates of the unrestrained nodes $\boldsymbol{z}$ are linear in the vertical coordinate of the abutments $\boldsymbol{z}_f$ and in the reciprocal variable $1/\bar{q}$. Methods of sequential convex programming are available that implement approximations of the objective functions and constraints in the direct or the reciprocal variable, depending on the sign of the gradient. The method of moving asymptotes by Svanberg (1987) is used in the numerical investigations.

The formulation in Eqn. (4) can be applied to grids with any topology and restraints. A single-layer network can be used to deal with unreinforced no-tension shell structures. An additional layer may be implemented to account for an underlying system of ribs, as detailed in Section 4.

3. A case study

This section introduces the case study, i.e. the stellar masonry vault originally built in the church of Tereske (Hungary). Some brief notes on the history of the ancient church and on the building material used in the site are provided. A description of the geometry of the vault is given, as well.

3.1 Some brief historical notes

Tereske is an Árpádian settlement in Nógrád county, Hungary. The Benedictine abbey of Tereske was firstly mentioned in historical writings that date back to 1219, even though its construction is probably earlier. The Varadinum Register (Borovszky and Karácsonyi, 1903) reports the existence of a monastery in the settlement of Triska, but neither the founding time of the monastery, nor the identity of the founder, remained. Large archeological excavations that were operated in the 1960s allowed reconstructing the long history of the building, see e.g. Mag Hella (2014). Indeed, history has played a significant role in the area, also affecting the life of the monastery and the transformation of the construction, see Figure 1.

The earliest church was probably a single nave block without any tower, originally built in the Romanesque style. As documented in Czaich (1903), the church was re-built in the Gothic style in the 1490s, in connection with a fire. In the 16th century, the area was occupied by the Ottomans and only liberated in the early 17th century. During this period, the building was used as a mosque.

The stellar masonry vault investigated in this work was originally built in the Gothic period at the end of the single nave, over the chancel. Even though it was destroyed in the first half of the 20th century, the several remainings of the stone ribs that were found during the excavations and the prints of the brick masonry webs that are still visible in the perimetral walls, allowed for a detailed reconstruction of its geometry (Pálos, 2010).

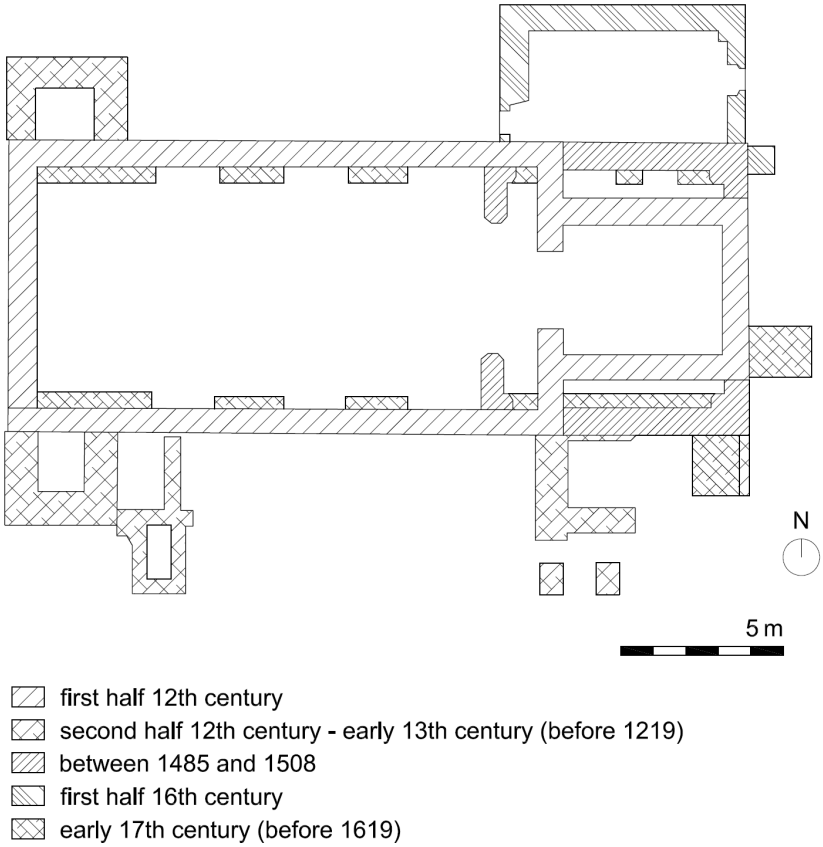

Figure 1: Schematic floor plan of the church according to archeological drawings reported by Mag Hella (2014).

Figure 2 - Re-construction works: a view of the re-built stellar vault (left); reproduction of the keystone at the highest intersection of the ribs (right).

Reconstruction works are currently being performed to re-build the vault by using restored remainings of the stone ribs along with reproductions of the missing parts, see Figure 2. Restauration works started with the collection of the remaining parts of the ribs and the analysis of their stone to find appropriate materials for the missing portions. These stones have been recently used to reconstruct the ribs using an ad hoc scaffolding, whereas a new webbing covered by plaster has been added upon, following the geometry reported in Pálos (2010). Both the walls and ribs of the vault were built using the sandstone of Hárshegy formation. This loess was formed in the early Oligocene, about 30 million years ago, in a shallow marine environment (littoral and shallow sublittoral, with reduced saltwater and lagoon in the lower part). The yellow, reddish-brown, or grayish-colored rock is composed almost entirely of quartz grains of sand or fine gravel, but in some places contains deposits of refractory clay and coal. The gravel material of the rock is of metamorphic and igneous origin. Its binder is mostly siliceous, making Hárshegy sandstone a relatively hard and durable rock which was an appreciated building material across the time, see Vattai and Rozgonyi-Boissinot (2018).

3.2 Geometry of the stellar vault

A plan view of the stellar vault is represented in Figure 3, whereas a simplified three-dimensional model is sketched in Figure 4, along with a lateral view. A section of the stellar vault at the crown is given in Figure 5, which shows a detail of the stone ribs and the overlying webbing. Due to the limited thickness of the masonry webbing, ribs are expected to play a crucial role in the equilibrium of this vault.

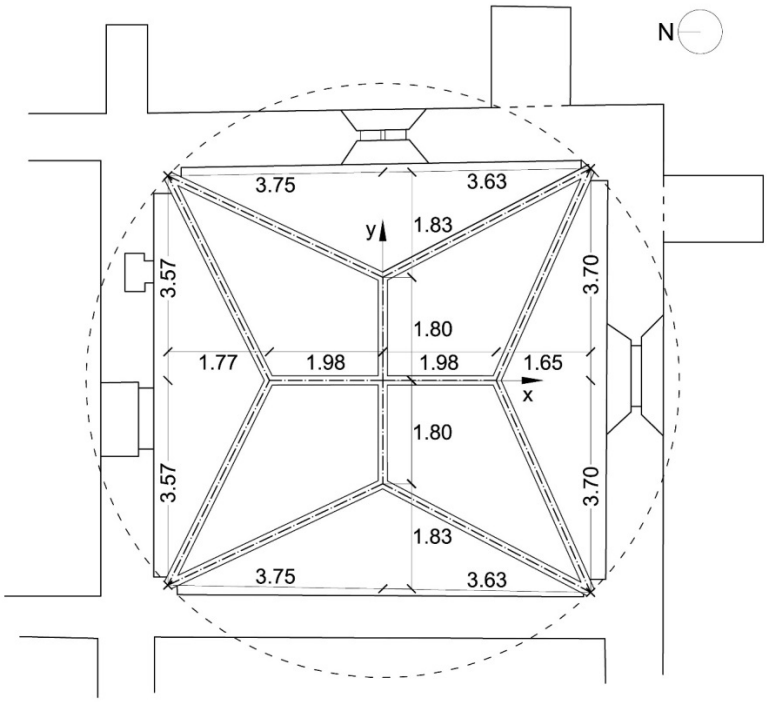

Figure 3 - Plan view of the stellar vault (dimensions are in m).

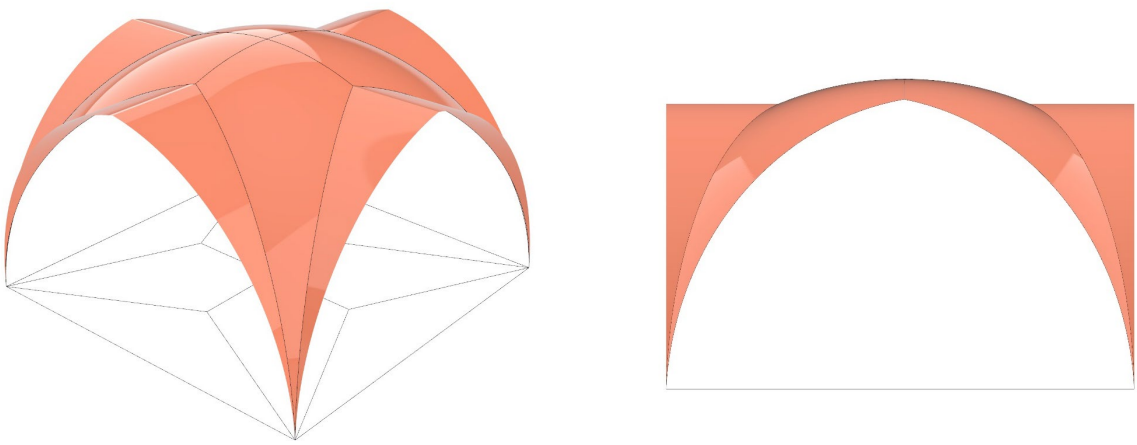

(a) (b)

Figure 4 - A three-dimensional view (a) and a lateral view (b) of the stellar vault.

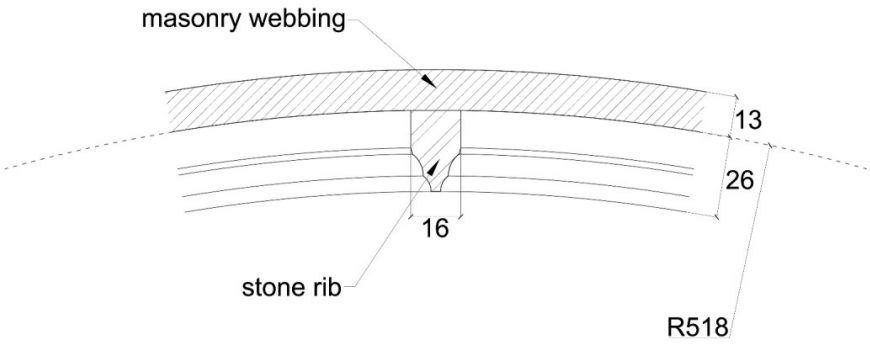

Figure 5 - Section of the stellar vault at the keystone (dimensions are in cm).

A cartesian reference system is adopted to describe the vault, assuming as elevation zero (impost level) the top of the four piers that receive the vertical loads at the corners, see Figure 3. The covered bay is slightly asymmetric. Indeed, the vault spans 7.38 m along the *x* axis, i.e. the N-S direction, whereas 7.26 m along the *y* axis, i.e. the W-E direction (which is the main axis of the nave). The central part of the vault, i.e. the region inscribed within the eight inclined ribs, is modelled on a spherical surface, whereas the four lateral segments are simple curve systems. The circle represented in Figure 3 stands for the intersection of the spherical surface used to model the intrados of the masonry webbing with the impost plane (at elevation zero). The sphere has radius R=5.18 m and centre in O (0, 0, -0.30 m). The groins lie at the intersection of this sphere with the eight vertical planes that contain the star-shaped projection of the ribs onto the horizontal plane represented in Figure 3. This set of curves defines the extrados of the inclined ribs, see Figure 5. The intrados of the four segments of the vault can be sketched by extruding these lines along the *x* or the *y* direction. Indeed, the section of the segments along the perimetral wall is made by pointed arches. A transversal and a longitudinal rib are added in the central part of the vault, following the curvature of the sphere. Unlike more complex stellar vaults with tiercerons and liernes, no diagonal or wall rib is reported, see Kulig and Romaniak (2007).

4. *Numerical investigations*

Funicular analyses are used to investigate the equilibrium of the stellar vault under self-weight, adopting two different assumptions in the modelling of the ribs. At first all the members of the funicular network are assumed to belong to a one-layer grid. Subsequently, a two-layer grid is adopted with the aim of modelling the ribs separately. In the latter case, vertical members are introduced to allow the load pass from the upper layer (masonry webbing) to the lower one (stone ribs). To avoid the arising of vertical members with zero length, which means infinite force densities, the bounds assigned to the nodes of the lower layer are shifted downwards by a given amount, with no effect on the equilibrium in the case of vertical loads. Alternatively, a minimum gap could be enforced by selecting a suitable set of lower and upper bounds for the coordinates of the extremal nodes of these elements.

The four corner nodes of the one-layer network are fully restrained. In the two-layer network, only the four corner nodes connecting the ribs to the ground are fully restrained. In both cases, each one of the perimetral nodes is restrained only in the direction that is orthogonal to the plane of the adjacent wall: more in details, the perimetral nodes of the N and S webs are restrained only along the *x* direction, whereas those of the E and W webs only along the *y* direction.

The specific gravity of the masonry webbing is assumed as γ_w = 18 kN/m^3, whereas the weight of the rib, per unit length, is taken as 0.75 kN/m (corresponding to a specific gravity of the stone rib equal to γ_r = 23.5 kN/m^3). Point forces are evaluated by computing the tributary area and length of each node of the network, using the mid-surface of the vault to derive the relevant elevations.

4.1 One-layer funicular networks

The fixed plan geometry adopted for the generation of a one-layer network for the

funicular analysis of the stellar vault is represented in Figure 6. A few members lie along the projection of the inclined ribs. Their nodes are connected both to branches in the segments, which lie along their principal directions of curvature, and to elements in the central web, which connect nodes lying at similar height. Additionally, a few branches are used to model the longitudinal and transversal ribs and provide a possible load path in the central web towards the four corners. Reference is made e.g. to Roca et al. (2019) and Como (2016) for review and discussion on the definition of discrete load paths to perform the funicular analysis of curved structures. Apart from the branches following the geometry of the ribs, the network in Figure 6 allows forces to flow along paths that have been mainly inspired by the principal directions of curvature of the surfaces (see the lateral segments of the webbing) along with the expected load transfers towards the imposts (see the spherical part of the webbing). As reported in the above-mentioned reviews, such kind of grids has been largely used in the literature. However, it must be remarked that the choice of the grid largely affects the quality of the achieved solutions, since it defines the design domain in which admissible solutions are sought. Reference is made to Block and Lachauer (2014a) for a detailed discussion on the topic.

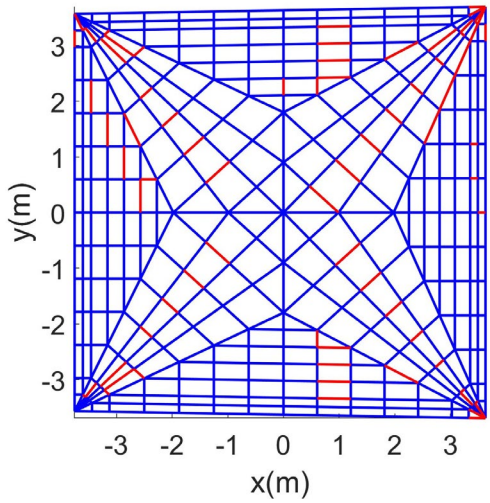

Figure 6 - Fixed plan geometry of a one-layer network to analyze the stellar vault (independent branches are marked in red).

The analysis of the augmented matrix governing the horizontal equilibrium, i.e. the matrix obtained by appending the coefficients and the constant terms of the linear system in Eqn. (1), points out that there exist 74 independent force densities out of 704. The branches belonging to the set used in the simulation are marked in red in Figure 6. It must be remarked that this set is not unique. It depends on the result of a Gauss-Jordan elimination procedure that is performed on the linear system in Eqn. (1). Alternative sets of independent unknowns can be generated for the same grid by changing the numbering of the branches and running again the Gauss-Jordan elimination procedure. Such kind of numerical tests have been performed in Bruggi (2020), addressing the funicular analysis of a groin vault under vertical loads. The same solution was retrieved in all the simulations, whereas a limited variability was observed in terms of number of iterations to achieve convergence.

The optimization problem of Eqn. (4) is set up in terms of 78 parameters (74 independent force densities and the height of four nodes restrained along the vertical direction, at the corners). Assuming the intrados of the masonry webbing as the

reference level, the nodes located along the ribs are enforced to lie within the interval [-21, +13] cm, whereas [0, +13] cm is used elsewhere, see Figure 5. Indeed, due to the peculiar shape of their cross-section, a reduced height has been considered for the ribs in the numerical simulations.

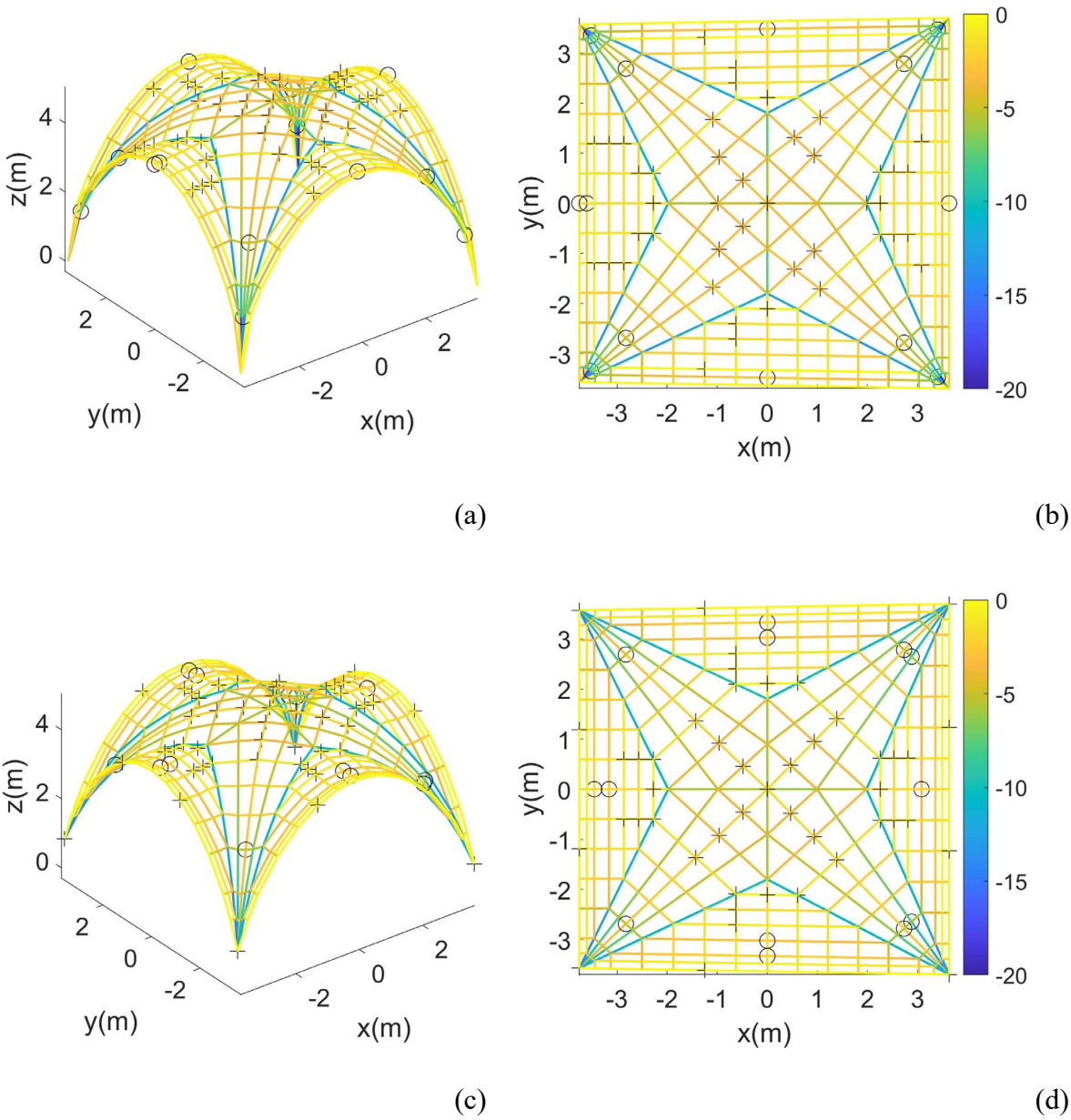

Figure 7 – One-layer funicular networks minimizing the horizontal reactions at: all the perimetral nodes (a-b); all the perimetral nodes, except the corners (c-d) (element forces are in kN).

Network of minimum thurst at:	*objective function*	$R_{z,max}$	$R_{x,max}$	$R_{y,max}$	F_{max}
all the perimetral nodes	35.73 (29.16)	49.80	7.13	7.85	19.21
all the perimetral nodes, except the corners	18.26	49.80	14.64	15.38	14.51

Table 1 - Maximum reactions in the z, x, y direction ($R_{z,max}$ $R_{x,max}$ $R_{y,max}$, respectively) and maximum element forces (F_{max}) in the single-layer funicular networks of Figures 7 (values in kN).

A preliminary investigation addresses the selection of the objective function. The pictures (a) and (b) in Figure 7 refer to the funicular network achieved by minimizing the sum of the horizontal components all along the perimeter of the vault; the pictures (c) and (d) concern the minimization of the horizontal reactions considering all the perimetral nodes, except those at the four corners. As introduced in Section 2, in the former case the minimization of the (squared) sum of the thrusts should relieve the four corners at the cost of non-negligible out-of-plane horizontal actions acting on the perimetral walls. Conversely, in the latter case it is expected that most of the thrust is localized at the four imposts, where vertical forces flow to the underlying supports and suitable lateral stiffness is provided in both directions (due to the geometry of the intersecting walls). Effects of such kind of assumptions on the features of the achieved funicular networks are reviewed next.

In both cases, the algorithm succeeds in finding solutions that lie within the geometry of the vault. The symbols "+" and "°" stand for points where the nodes of the single-layer funicular network touch the extrados and the intrados of the existing envelope, respectively. Table 1 reports the maximum values of the component of the reactions at the restrained nodes, along with the maximum compressive forces in the branches, for each one of the two computed networks. At convergence, the implemented objective function reads 35.73 kN in the former case, and 18.26 kN in the latter.

The achieved solutions are slightly asymmetric, due to the lack of symmetry in the analysed geometry. In both cases, the branches along the inclined ribs are those subjected to the biggest forces, whereas the four segments undergo the smallest ones. Independently of the objective function, the achieved funicular networks touch the extrados around the crown and in the regions where the segments intersect the central sphere. Both approach the intrados along the diagonal, not far from the imposts, and in the lateral segments in the vicinity of the middle of the perimetral sides.

As expected, a substantial difference arises at the imposts. The adoption of an objective function that includes the thrusts of all the perimetral nodes calls for a deep funicular network, see Figure 7(a), thus minimizing the main horizontal forces arising at the corners. When these four nodes are excluded from the computation of the objective function, a shallower solution arises to minimize the thrusts over the perimetral walls. According to Table 1, the maximum values of the component of the horizontal reactions (at the corners) in the latter case are approximately double those in the former. Conversely, evaluating the objective function that excludes corner contributions at convergence, a much bigger value is found for the network in Figure 7 (a-b) (29.16 kN vs. 18.26 kN). According to Figure 7(b) and Figure 7(d) the highest thrusts acting over the lateral walls arise in the vicinity of the imposts. However, their intensity is much lower in the latter case. In this funicular network, the load path at the impost is such that almost all the branches converging to the corners are remarkably stressed (along the ribs and in the inner web). The maximum value of the force in the elements read in Figure 7(d) is less than that read in the ribs in Figure 7(b).

In the simulations presented next, the minimization of the horizontal thrust is performed including in the objective function all the perimetral nodes except the corner ones.

4.2 Two-layer funicular networks

The fixed plan geometry shown in Figure 6 is modified to account for the emerging ribs separately, by means of two-layer funicular networks. Indeed, the 64 branches lying along the ribs of the grid in Figure 6 are doubled to generate an additional underlying layer. The new 56 nodes are connected to those of the overlying layer by means of the same number of vertical branches. The analysis of the augmented matrix that governs the horizontal equilibrium of the nodes, see Eqn. (1), points out that there exist 74 independent force densities out of 704 in the overlying layer (they are the same as those marked in red in Figure 6), 2 out of 64 independent branches in the underlying layer, and 61 out of 61 independent force densities in the added vertical members. Hence, the optimization problem of Eqn. (4) is set up in terms of 141 parameters (137 force densities and the height of the four nodes restrained along the vertical direction). Assuming the intrados of the masonry webbing as the reference level, the nodes belonging to the upper layer are enforced to lie within the interval [0, +13], whereas [-21, 0] cm is used for the underlying rib layer (see Figure 5).

Figure 8(a) shows a general view of the network achieved via the multi-constrained minimization of the thrusts along the perimetral walls: blue branches refers to the rib layer, whereas thick black branches are elements belonging to the overlying webbing layer. Thin vertical elements represent the branches connecting the two layers. Figure 8(b) and (c) report maps of the stresses in the overlying and underlying layers, respectively. The symbols “+” and “°” stand for points where the nodes of the two-layer funicular network reach the allowable upper or lower limit, respectively.

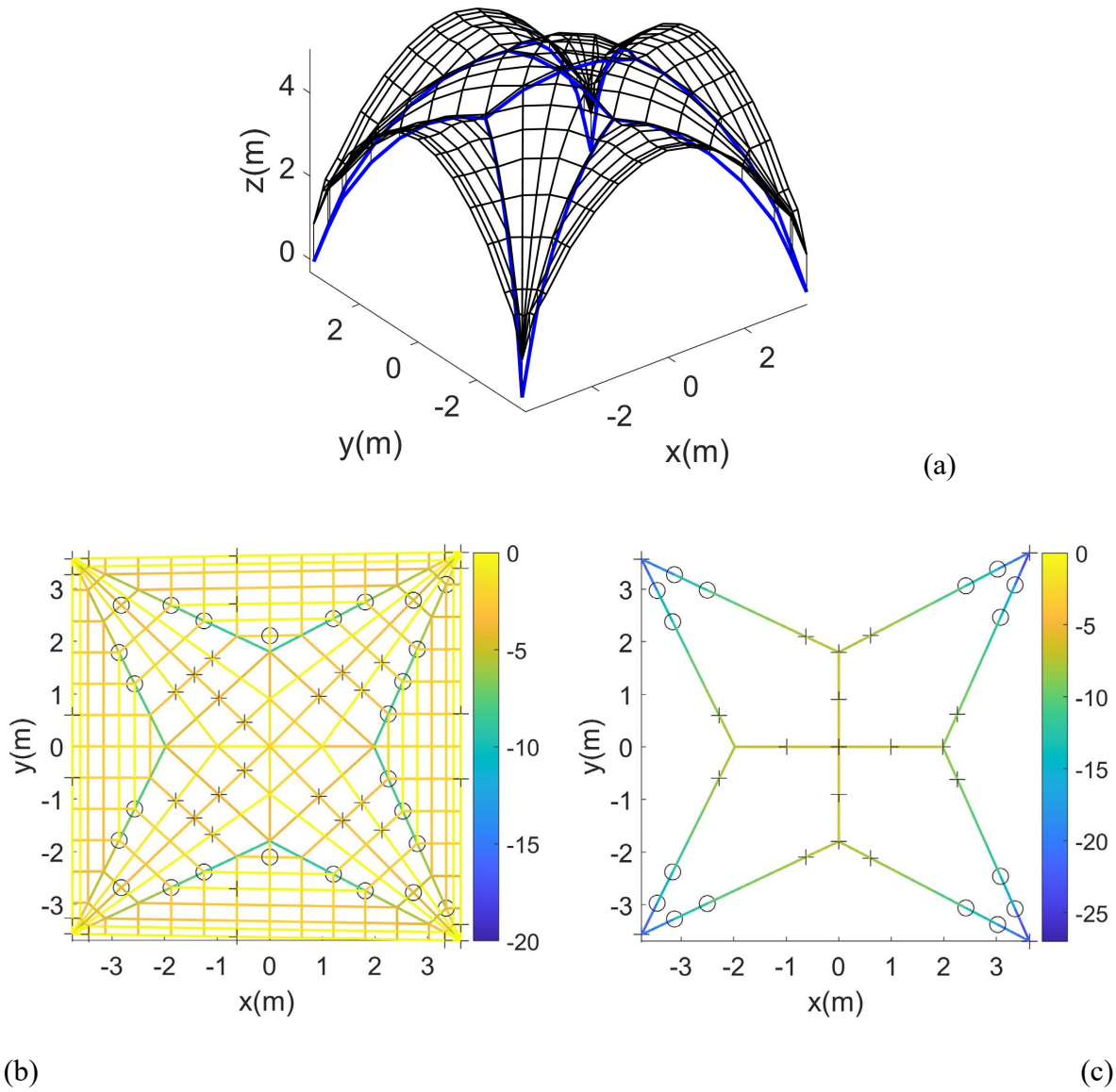

Figure 8 – Two-layer funicular network (with 141 parameters): overall view (a); overlying layer - webbing (b); underlying layer - ribs (element forces are in kN).

Network with:	*objective function*	$R_{z,max}$	$R_{x,max}$	$R_{y,max}$	F_{max}	
					webbing	*ribs*
141 parameters	21.02	49.81	9.84	10.95	8.83	23.57
221 parameters	17.18	49.86	10.75	11.91	6.84	26.37

Table 2- Maximum reactions in the z, x, y direction ($R_{z,max}$ $R_{x,max}$ $R_{y,max}$, respectively) and maximum element forces (F_{max}) in the two-layer funicular networks of Figures 8 and 10 (values in kN).

Table 2 reports maximum reactions and element forces in both webbing and ribs. At convergence, the objective function of the achieved two-layer funicular network is approximately 15% bigger than that of the one-layer network in Figure 7 (c-d). However, the components of the maximal horizontal reactions (read at the corners) are remarkably lower (around 30%) in the case of the two-layer network. At the impost, the funicular polygon arising in the ribs, see Figure 8(a), is much deeper than the branches of the network in Figure 7(c).

The overlying layer represented in Figure 8(b) touches the extrados of the webbing around the crown, as similarly observed in Figure 7(c). Differently, it touches the intrados of the webbing mainly along the inclined ribs. Referring to the underlying layer of the ribs, see Figure 8(c), the achieved solutions recall the equilibrium of arches where the funicular polygon touches the extrados at the crown and the intrados next to the haunches. Looking at the distribution of the element forces in the different sets of branches of the two-layer network, it may be concluded that the ribs are more stressed than the overlying webbing, except for the regions at the intersection of the inclined ribs with the transversal or the longitudinal ones. The maximum force read in the webbing is much lower than that read in the ribs. Also, the maximum force that the ribs undergo in the two-layer network is remarkably bigger than that arising at the impost of the single-layer network in Figure 7 (c-d). It must be remarked that this is in spite of the fact that, at the impost, the funicular polygons in the ribs of the two-layer network are deeper than the one-layer network.

A refined version of the two-layer funicular networks is finally considered. As reported in Section 4.1, the original grid was largely inspired by the geometry of the ribs and the principal directions of curvature of the segments of the webbings. Principal directions

are not uniquely defined in the spherical part, where maximum and minimum curvatures are achieved along any direction. Additional load paths may be conveniently provided in this region by adding a set of new members within the existing nodes of the webbing layer, see Figure 9. Indeed, the degree of indeterminacy of the new network is higher and the number of minimization unknowns rises to 221, approximately one and a half times than for the grid represented in Figure 6.

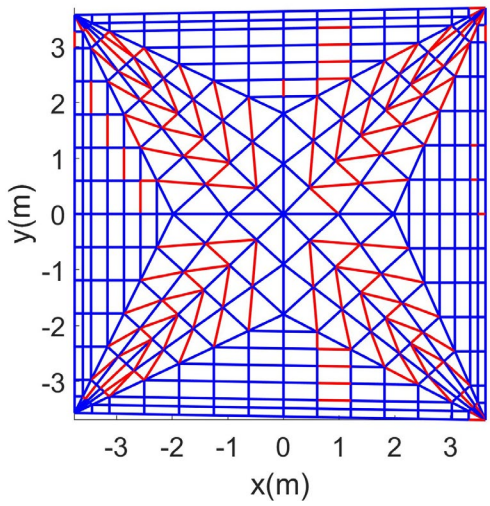

Figure 9 - Fixed plan geometry of a refined two-layer network to analyze the stellar vault (overlying layer, independent branches marked in red).

The achieved funicular network is represented in Figure 10. The extended design domain allows capturing an improved solution in terms of objective function, which is 20% less than in the previous case, being also the best result among those herein reported. The thrust over the lateral walls decreases at the cost of an increase of less than 10% in the maximum reactions at the corners. A few variations may be observed when looking at the points where the network touches the intrados or the extrados of the webbing/ribs, see Figure 10 (b) and (c), in comparison with those found for the less articulated network, see Figure 8 (b) and (c). The difference between the maximum values of the element forces in the overlying layer and in the underlying one is much

sharper in the articulated network than in the previous one. According to values reported in Table 2, ribs are much more stressed than branches in the webbing. Indeed, this refined solution confirms that ribs play an important role in the statics of the considered vault.

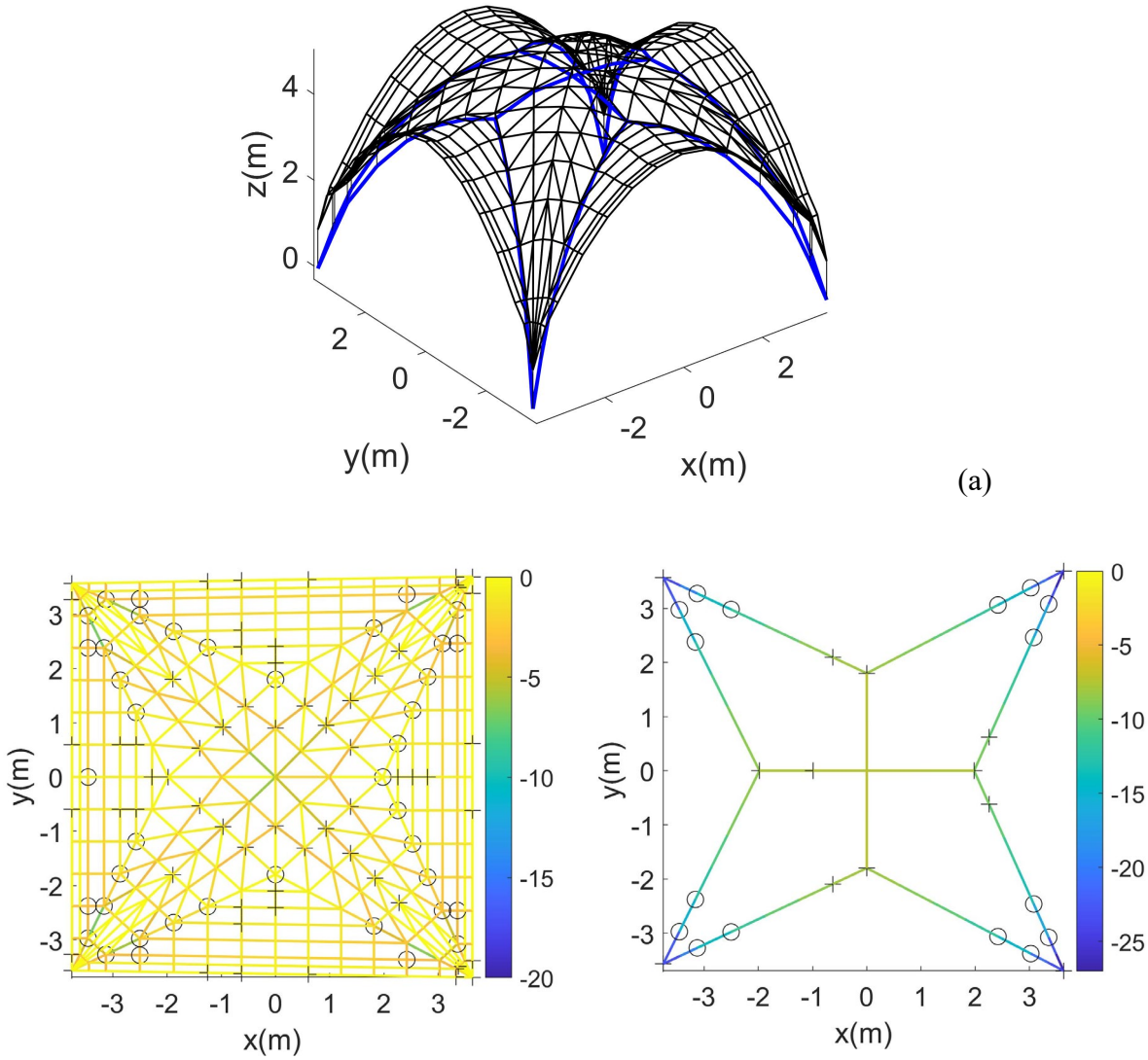

Figure 10 - Two-layer funicular network (with 221 parameters): overall view (a); overlying layer - webbing (b); underlying layer - ribs (element forces are in kN).

It must be remarked that the achieved force networks should be regarded as statically admissible solutions that strongly depend on the geometry of the initial grid. To

approximate the real state of stress in the vault, i.e. to perform a consistent analysis of the curved structure, load paths allowed by the branches of the network should also account for the observed crack pattern, see O'Dwyer (1999) and Baratta and Corbi (2011). Due to the lack of this information in the considered case, other analytical and numerical approaches of analysis could be conveniently used to derive grids that can achieve more accurate networks.

5. Conclusions

The adoption of two-layer spatial networks in the funicular analysis of ribbed masonry vaults has been addressed, adopting a multi-constrained optimization framework to minimize the thrusts. The implemented algorithm selects anti-funicular networks with given plan geometry that are in equilibrium with the loading and fulfil local constraints on the height of the nodes and on the sign of the force densities. The method can handle partial and full restraints, as well as grids with general topology. Two-layer spatial networks may be investigated to account for the load path in the overlying webbing and in the supporting ribs, as reported for the stellar masonry vault originally built in an ancient Hungarian church.

Networks with different topology and number of elements have been considered in the numerical simulations, adopting two types of objective functions. In all the cases, systems of forces that are fully feasible with the geometrical and no-tension constraints have been found. By minimizing the sum of the horizontal components of the reactions all along the perimeter of the vault, non-negligible thrusts arise not only at the imposts but also in their vicinity. Conversely, by excluding the four corner nodes from the evaluation of the objective function, higher values of the thrust are localized at the corners, in conjunction with shallower networks. The achieved results are affected by the topology of the grid, i.e. the fixed plan projection used in the simulation: by

adopting finer meshes, enlarged design domains are made available to the minimizer for an improvement of the objective function; by changing the number of layers in the network, new design problems are set up that can disclose other load paths.

At first, a single-layer network has been implemented to assess the method with the two types of objective function. In the achieved funicular networks, the most stressed elements are those located at the intersection of the four segments with the central spherical part, i.e. where the ribs lie. A new grid for the investigation of two-layer networks has been derived by doubling nodes and elements along the rib and introducing branches between the overlying layer (representing the webbing) and the underlying one (standing for the ribs). A refined version has been implemented as well, to allow for additional load paths. Especially in the last case, the elements in the webbing undergo forces that are much lower than those found in the ribs, suggesting that ribs play an important statical role in the equilibrium of the considered stellar vault. This is in agreement with results of the recent literature dealing with the structural analysis of ribbed vaults through numerical methods.

One-layer and two-layer funicular networks can be conveniently investigated to generate a set of statically admissible solutions. As suggested e.g. by O'Dwyer (1999), preferred grids are those consistent with the stress regime expected in the masonry vault. Such kind of grids could be generated after preliminary finite element analysis accounting for a limited strength in tension of the material, see in particular Angelillo et al. (2010) and Briccola and Bruggi (2019), as currently under investigation. Also, effective networks could be retrieved removing some of the classical assumptions used in the derivation of funicular networks, i.e. working with prescribed values of compressive strength and friction, see D'Ayala and Tomasoni (2011). To this goal, the proposed multi-constrained formulation could be endowed with enforcements on the

maximum compressive force allowed in the branches of the network, as well as geometrical constraints controlling the deviation of the direction of each force with respect to the normal to an assigned contact surface. The achieved results could be compared with available numerical approaches for historical masonry construction that also account for finite compression and friction strength. Reference is made to the discrete element model in Lemos (2007) and Gobbin et al. (2020), the rigid block model for collapse mechanism analysis in Cascioli et al. (2020), the unified formulation for non-linear time history, static pushover and limit analysis that is implemented in Portioli (2020) by means of mathematical programming.

Acknowledgments

Attila Holman, owner and chief civil eng. at Confector Ltd, Hungary, who supported the restoration works, is gratefully acknowledged for the inspiring discussions on the assessment of the vault.

The financial support of TKP2020 Institution Excellence Subprogram, Grant No. TKP2020 BME-IKA-VÍZ of the National Research Development and Innovation Office of Hungary is acknowledged.

References

Andreu, A., Gil, L., & Roca, P. (2007). Computational analysis of masonry structures with a funicular model. *Journal of Engineering Mechanics, 133*(4), 473-480. doi:10.1061/(ASCE)0733-9399(2007)133:4(473)

Angelillo, M., Babilio, E., & Fortunato, A. (2013). Singular stress fields for masonry-like vaults. *Continuum Mechanics and Thermodynamics, 25*(2-4), 423-441. doi:10.1007/s00161-012-0270-9

Angelillo, M., Cardamone, L., & Fortunato, A. (2010). A numerical model for masonry-like structures. *Journal of Mechanics of Materials and Structures, 5*(4), 583-615. doi:10.2140/jomms.2010.5.583

Angelillo, M., Fortunato, A., Montanino, A., & Lippiello, M. (2014). Singular stress fields in masonry structures: Derand was right. *Meccanica, 49*(5), 1243-1262. doi:10.1007/s11012-014-9880-6

Baratta, A., & Corbi, O. (2011). On the statics of no-tension masonry-like vaults and shells: Solution domains, operative treatment and numerical validation. *Annals of Solid and Structural Mechanics*, 2(2-4), 107-122. doi:10.1007/s12356-011-0022-8

Beatini, V., Royer-Carfagni, G., & Tasora, A. (2018). The role of frictional contact of constituent blocks on the stability of masonry domes. *Proceedings of the Royal Society A: Mathematical, Physical and Engineering Sciences*, 474(2209), 20170740. doi:10.1098/rspa.2017.0740

Bertolesi, E., Adam, J. M., Rinaudo, P., & Calderón, P. A. (2019). Research and practice on masonry cross vaults – A review. *Engineering Structures,* 180, 67-88. doi:10.1016/j.engstruct.2018.10.085

Block, P., & Lachauer, L. (2014a). Three-dimensional (3D) equilibrium analysis of gothic masonry vaults. *International Journal of Architectural Heritage*, 8(3), 312-335. doi:10.1080/15583058.2013.826301

Block, P., & Lachauer, L. (2014b). Three-dimensional funicular analysis of masonry vaults. *Mechanics Research Communications*, 56, 53-60. doi:10.1016/j.mechrescom.2013.11.010

Block, P., & Ochsendorf, J. (2007). Thrust network analysis: A new methodology for three-dimensional equilibrium. *Journal of the International Association for Shell and Spatial Structures, 48*(155), 167-173

Borovszky, & S., Karácsonyi, J. (1903). Regestrum varadinense examinum ferri candentis ordine chronologico digestum, descripta effigie editionis a. 1550 illustratum, sumptibusque Capituli varadinensis lat. rit. Curis et laboribus Joannis Karácsonyi et Samuelis Borovszky ... editum. Budapest: Typis V. Hornyánsky (in Latin)

Briccola, D., & Bruggi, M. (2019). Analysis of 3D linear elastic masonry-like structures through the API of a finite element software. *Advances in Engineering Software, 133*, 60-75. doi:10.1016/j.advengsoft.2019.04.009

Bruggi, M. (2020). A constrained force density method for the funicular analysis and design of arches, domes and vaults. *International Journal of Solids and Structures*, 193-194, 251-269. doi:10.1016/j.ijsolstr.2020.02.030

Cascini, L., Gagliardo, R., & Portioli, F. (2020). LiABlock_3D: A software tool for collapse mechanism analysis of historic masonry structures. *International Journal of Architectural Heritage*, 14(1), 75-94. doi:10.1080/15583058.2018.1509155

Cercadillo-García, C., & Fernández-Cabo, J. L. (2016). Analytical and numerical funicular analysis by means of the parametric force density method. *Journal of Applied Research and Technology, 14*(2), 108-124. doi:10.1016/j.jart.2016.03.001

Chen, S., & Bagi, K. (2020). Crosswise tensile resistance of masonry patterns due to contact friction. *Proceedings of the Royal Society A*, 476(2240), 20200439. doi: 10.1098/rspa.2020.0439

Christensen, P. W., & Klarbring, A. (2008). An introduction to structural optimization, Springer

Como, M. (2016). Statics of Historic Masonry Constructions, Springer

Czaich Á. G. (1903) Regesták VIII. Incze pápa korából 1484-1492, - Regestas from the time of Pope VIII. Incze 1484-1492, Budapest (in Hungarian)

D'Altri, A. M., Sarhosis, V., Milani, G., Rots, J., Cattari, S., Lagomarsino, S., Sacco, E., Tralli, A., Castellazzi, G., de Miranda, S. (2019). Modeling strategies for the computational analysis of unreinforced masonry structures: Review and classification. *Archives of Computational Methods in Engineering, 27*(4), 1153-1185. doi:10.1007/s11831-019-09351-x

D'Ayala, D. F., & Tomasoni, E. (2011). Three-dimensional analysis of masonry vaults using limit state analysis with finite friction. *International Journal of Architectural Heritage, 5*(2), 140-171. doi:10.1080/15583050903367595

Di Pasquale, S. (1996). L'Arte del Costruire, tra conoscenza e scienza, Marsilio (in Italian).

Fraddosio, A., Lepore, N., & Piccioni, M. D. (2020). Thrust surface method: An innovative approach for the three-dimensional lower bound limit analysis of masonry vaults. *Engineering Structures*, 202 doi:10.1016/j.engstruct.2019.109846

Fraternali, F. (2010). A thrust network approach to the equilibrium problem of unreinforced masonry vaults via polyhedral stress functions. *Mechanics Research Communications, 37*(2), 198-204. doi:10.1016/j.mechrescom.2009.12.010

Gyalog L., & Síkhegyi F. (2005). Geological map of Hungary, Publication of the Hungarian State Geological Institute, Budapest. https://map.mbfsz.gov.hu/fdt100/

Gobbin, F., de Felice, G., & Lemos, J. V. (2020). A discrete element model for masonry vaults strengthened with externally bonded reinforcement. *International Journal of Architectural Heritage*, doi:10.1080/15583058.2020.1743792

Grillanda, N., Chiozzi, A., Bondi, F., Tralli, A., Manconi, F., Stochino, F., & Cazzani, A. (2019). Numerical insights on the structural assessment of historical masonry stellar vaults: The case of Santa Maria del Monte in Cagliari. *Continuum Mechanics and Thermodynamics,* doi:10.1007/s00161-019-00752-8

Heyman, J. (1966). The stone skeleton. *International Journal of Solids and Structures*, 2 (2), 249–279. doi:10.1016/0020-7683(66)90018-7

Kulig, A., & Romaniak, K. (2007). Geometrical models of stellar vaults. *The Journal of Polish Society for Geometry and Engineering Graphics*, 17, 51-56.

Lemos, J. V. (2007). Discrete element modeling of masonry structures. *International Journal of Architectural Heritage*, 1(2), 190-213. doi:10.1080/15583050601176868

Lengyel, G., & Bagi, K. (2015). Numerical analysis of the mechanical role of the ribs in groin vaults. *Computers and Structures, 158*, 42-60. doi:10.1016/j.compstruc.2015.05.032

Mag Hella (2014). Tereske temploma a késő középkorban. - Church of Tereske in the late Middle Ages- *Archeologia - Altum Castrum Online Magazin*. Last retrieved on 12/06/2020 at www.archeologia.hu (in Hungarian).

Marmo, F., & Rosati, L. (2017). Reformulation and extension of the thrust network analysis. *Computers and Structures*, 182, 104-118. doi:10.1016/j.compstruc.2016.11.016

Marmo, F., Masi, D., & Rosati, L. (2018). Thrust network analysis of masonry helical staircases. *International Journal of Architectural Heritage, 12*(5), 828-848. doi:10.1080/15583058.2017.1419313

Marmo, F., Ruggieri, N., Toraldo, F., & Rosati, L. (2019). Historical study and static assessment of an innovative vaulting technique of the 19th century. *International Journal of Architectural Heritage, 13*(6), 799-819. doi:10.1080/15583058.2018.1476607

Milani, E., Milani, G., & Tralli, A. (2008). Limit analysis of masonry vaults by means of curved shell finite elements and homogenization. *International Journal of Solids and Structures*, 45(20), 5258-5288. doi:10.1016/j.ijsolstr.2008.05.019

Mousavian, E., & Casapulla, C. (2020). The role of different sliding resistances in limit analysis of hemispherical masonry domes. *Frattura ed Integrità Strutturale*, 14(51), 336-355. doi:10.3221/IGF-ESIS.51.25.

O'Dwyer, D. (1999). Funicular analysis of masonry vaults. *Computers and Structures*, 73(1-5), 187-197. doi:10.1016/S0045-7949(98)00279-X

Pálos, F. (2010). A tereskei templom, -Church of Tereske-, Aszód (in Hungarian).

Pellegrino, S., & Calladine, C. R. (1986). Matrix analysis of statically and kinematically indeterminate frameworks. *International Journal of Solids and Structures*, 22(4), 409-428. doi:10.1016/0020-7683(86)90014-4

Portioli, F. P. A. (2020). Rigid block modelling of historic masonry structures using mathematical programming: A unified formulation for non-linear time history, static pushover and limit equilibrium analysis. *Bulletin of Earthquake Engineering*, 18(1), 211-239. doi:10.1007/s10518-019-00722-0

Roca, P., Cervera, M., Gariup, G., & Pela', L. (2010). Structural analysis of masonry historical constructions. classical and advanced approaches. *Archives of Computational Methods in Engineering, 17*(3), 299-325. doi:10.1007/s11831-010-9046-1

Roca, P., Lourenço, P., Gaetani, A. (2019). Historic Construction and Conservation: Materials, Systems and Damage, Taylor & Francis

Schek, H. (1974). The force density method for form finding and computation of general networks. *Computer Methods in Applied Mechanics and Engineering*, 3(1), 115-134. doi:10.1016/0045-7825(74)90045-0

Svanberg, K. (1987). The method of moving asymptotes—a new method for structural optimization. *International Journal for Numerical Methods in Engineering, 24*(2), 359-373. doi:10.1002/nme.1620240207

Tralli, A., Alessandri, C., & Milani, G. (2014). Computational methods for masonry vaults: A review of recent results. *Open Civil Engineering Journal, 8*(1), 272-287. doi:10.2174/1874149501408010272

Vattai A., & Rozgonyi-Boissinot N. (2018) The effect of grain size, surface roughness, and joint compressive strength on shear strength along discontinuities of Hungarian sandstones. *Central European Geology*, 61(1), 34-49. doi:10.1556/24.61.2018.03